ACS Catalysis

Research Article

pubs.acs.org/acscatalysis

Trends in the Hydrogen Evolution Activity of Metal Carbide Catalysts

Ronald Michalsky,[†] Yin-Jia Zhang,[‡] and Andrew A. Peterson*[,†]

[†]School of Engineering and [‡]Department of Chemistry, Brown University, Providence, Rhode Island 02912, United States

Supporting Information

ABSTRACT: Metal carbide catalysts are alternative nonprecious electrode materials for electrochemical energy conversion devices, such as for H_2 fuel cells or electrolyzers. In this article, we report the experimental exchange current densities for the hydrogen evolution reaction (HER) on eight mono- and bimetallic carbide electrocatalysts and correlate the current densities to hydrogen binding energies that we have calculated via electronic structure computations. We find these materials to have activities higher than those of their parent metals and intermediate between the catalytic activities of the Pt group and early transition-metal surfaces. Increased HER activities on metal carbides relative to their parent metals can be understood with a 3-fold higher sensitivity of metal carbides to the coverage-induced weakening of hydrogen adsorption relative to metal surfaces. The trends presented here can be useful for the design of bimetallic carbide electrocatalysts.

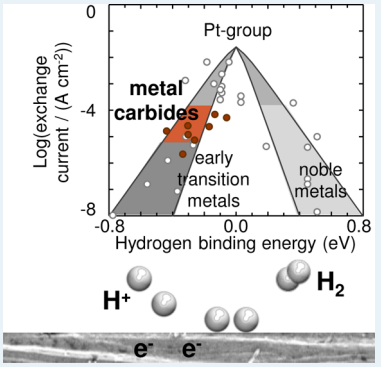

KEYWORDS: *electrocatalysis, surfaces, Sabatier principle, renewable energy, sustainable fuels*

The electrocatalytic hydrogen evolution reaction (HER), which is the reduction of aqueous protons by electrons passed through a catalyst to liberate H_2, is central to many electrochemical processes. When the electrical energy required to drive the reaction is derived from renewable or carbon-neutral resources such as photovoltaic electricity,[1] H_2 can serve as a carbon-neutral feedstock for the synthesis of ammonia,[2,3] as a reducing source for the deoxygenation of biofuels,[4] or as a fuel source for hydrogen fuel cells[5−7] for automotive[8] or stationary applications. In other electrochemical applications, the HER is a major side reaction that affects the product selectivity in electrocatalytic CO_2 reduction[9,10] or the local pH and the development of structural properties during metal electrodeposition.[11] The activity of an electrocatalytic surface to catalyze the HER, including monometallic surfaces and bimetallic metal overlayers, can be described by the strength of the hydrogen−surface bond; this has been shown in acidic[12,13] and alkaline[14] electrolytes. A so-called volcano plot[15] can be produced by plotting the exchange current density (i_0) for the HER versus the free energy of hydrogen adsorption ($\Delta G_B[H]$), yielding a peaked correlation with Pt or Pt-group composite materials at the top[12−14] at which hydrogen binds just strong enough to cover the surface but weak enough to facilitate desorption of the H_2 reaction product.[16] Beyond single-metal electrocatalysts, certain non-noble metal compounds and binary transition-metal alloys have been reported to catalyze the HER. The electrocatalytic activity of MoS_2 in the HER has been demonstrated to arise from the presence of edge sites at the metal sulfide surface, placing it near the top of the volcano,[17,18] while the activity of CuW alloys in catalyzing the HER and its reverse, the hydrogen oxidation reaction (HOR), is reportedly controlled by surface composition and surface coverage effects.[17−19] In this work, we studied metal carbide catalysts as alternative electrocatalysts for the HER and assessed the effect of hydrogen surface coverage on catalyst activity.

Certain carbides, such as those made from W and Mo, have been famously reported to exhibit catalytic activities that can be similar to that of Pt, especially for catalysis of the dissociation of H_2 in the presence of H_2O under ambient conditions[20] or catalysis of the HER.[21−23] However, the lack of a fundamental understanding of the catalytic activity of metal carbide surfaces has limited the rational design of carbide catalysts. In particular, the previously reported generally stronger hydrogen binding energies on transition-metal carbides[24−26] relative to those on their parent metals—which are already on the left, or strong-binding, side of the volcano for the HER—intuitively conflict with the enhanced activity for the HER on metal carbides.

In this work, we investigate the relation between the exchange current density for the HER measured with steady-state polarization experiments and the free energy of the hydrogen adsorbate determined from electronic structure calculations for a large number of transition-metal carbides as well as boron carbide. It will be shown that metal carbide surfaces are more susceptible to coverage effects, i.e., a weakening of hydrogen bonding due to the presence of other hydrogen adsorbates, than pure metals, which correlates with increased exchange current densities for the HER on metal carbides relative to the parent metal. Generally, we will show the activity of carbide catalysts in the HER to be intermediate between the low activities observed for early transition metals and the high activities observed for Pt-group metals. While this

Received: January 15, 2014
Revised: March 7, 2014
Published: March 12, 2014

   dx.doi.org/10.1021/cs500056u | ACS Catal. 2014, 4, 1274−1278

work focuses on the carbide electrocatalysts[27−30] for the HER, understanding hydrogen binding characteristics of metal carbide surfaces is useful in a variety of other catalytic processes, including CO_2 or CO reduction,[27,28,31−33] the water-gas-shift reaction,[34] steam reforming of methane,[35] and Fischer−Tropsch synthesis.[36]

HYDROGEN CHEMISORPTION ENERGIES

The binding strength of an adsorbate (A) at a surface can be calculated via electronic structure calculations and expressed as a binding energy, $\Delta E_B[A]$:

$$\Delta E_B[A] = E[\text{surface} + A] - (E[\text{surface}] + E[A]) \quad (1)$$

where E is the total electronic energy of a given geometric arrangement of atoms and $E[A]$ is a suitably chosen reference energy, taken to be half the energy of H_2 gas in the case of a hydrogen adsorbate. Figure 1 compares $\Delta E_B[H]$ values for

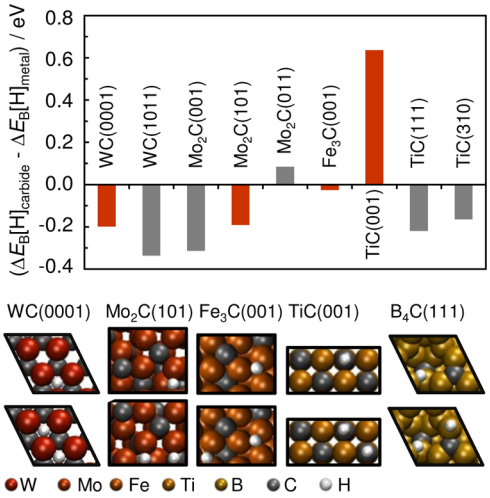

Figure 1. Difference in hydrogen adsorption energies on various metal carbide surfaces relative to their stepped parent metal surface.[25,26,38,39] The images below the graph, correlating to the red bars on the graph, show the optimal adsorption sites of H on selected metal carbide surfaces at either 1/4 [1/6 on $Fe_3C(001)$] ML_H (top row) or 1/2 [1/3 on $Fe_3C(001)$] ML_H (bottom row). Binding energies for Fe(211),[39] Mo(210),[26,38] and W(210)[26,38] are from the literature.

coverages of 1/6 to 1/4 monolayer hydrogen (ML_H) on various thermodynamically stable metal carbide surfaces to the equivalent values on the parent metal and shows generally, with few exceptions, stronger hydrogen chemisorption on metal carbides. This is in qualitative agreement with the previous work by Kitchin et al.[24] and does not change significantly when taking the closely packed fcc(111) or bcc(110) metal surface as a reference (Supporting Information). The deviation of $\Delta E_B[H]$ on TiC(001) can be explained by the tendency of reactive metals such as the early transition metals to form thermodynamically stable metal bulk compounds with highly anisotropic surface reactivities.[37]

To include coverage effects over a range of surface reactivities, we selected four carbide surfaces (colored red in Figure 1) in addition to $B_4C(111)$ and calculated the free energy of the hydrogen adsorption (i.e., $\Delta E_B[H]$ corrected for entropy and zero-point energies as described in the Supporting Information) at 1/6 to 1/2 ML_H. The optimized adsorption geometries are shown in Figure 1. Figure 2 shows the free energy diagram for the HER on metal carbides with various

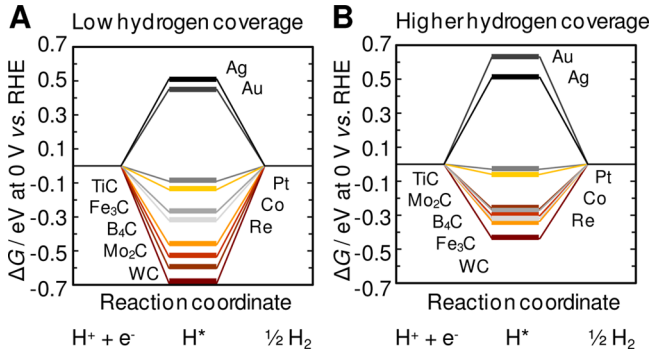

Figure 2. Free energy diagrams for the electrochemical reduction of H^+ at the equilibrium potential and under standard conditions (1 bar of H_2, pH 0, 298 K) on fcc(111) metal (gray lines)[12] and metal carbide surfaces (facets given in Figure 1; shown here as orange lines) at (A) low coverage, i.e., 1/4 ML_H on all surfaces (except 1/6 ML_H on Fe_3C), or (B) higher coverage, i.e., 1/2 ML_H on carbide surfaces (1/3 ML_H on Fe_3C) and 1 ML_H on metal surfaces. Negative ΔG values mark exergonic reaction steps.

transition-metal surfaces[12] included for reference. All energies are plotted at the reversible potential of the HER, such that the free energies per H atom (the chemical potential) of the initial and final states are zero.[40] An "ideal" catalyst would exhibit zero free energy change throughout the reaction.

With the exception of TiC(001), H adsorbs stronger to all studied metal carbide surfaces than to the transition-metal surfaces, which intuitively contradicts the reported activity of metal carbides for the HER. However, at increased hydrogen coverages, hydrogen binding on metal carbides becomes 3-fold weaker [from 0.08 eV on TiC(001) to 0.34 eV on $Mo_2C(101)$; average of 0.21 eV] than on metal surfaces [from 0.02 eV on Co(111) to 0.18 eV on Au(111); average of 0.07 eV]. This suggests the activity of metal carbides for the HER can be understood in terms of surface coverage, an effect that is well-known and for instance experimentally observed during the adsorption of CO on Ru(001).[41] We note the varying site preference of the H adsorbate on carbide surfaces indicates that the origin of these hydrogen binding characteristics is presumably of an electronic nature (rather than geometric), i.e., because of the interference of the additional adsorbates with the electronic states at the surface of the catalysts.

TRENDS IN THE EXCHANGE CURRENT DENSITY

To correlate the catalytic activity of metal carbides with the hydrogen chemisorption energy, we measured the exchange current density for the HER on eight metal carbide electrodes (Figure 3). All carbide electrodes are either dense metal carbide sheets (purchased), TiC nanoparticles supported on carbon fiber paper, or metals with an at-minimum several-micrometer thick layer of a polycrystalline carbide, as indicated by X-ray diffraction (XRD) before and after abrasive surface treatment and scanning electron microscopy (SEM) (Figure 3A,B). The unsteady baseline of the XRD pattern is due to integration of the intensity count recorded with a two-dimensional goniometer that was arrested at three or four fixed detector angles. The exchange current density was determined from steady-state polarization experiments (Figure 3C) used for the construction of Tafel plots (Figure 3D). Further experimental details and tabulated results are given in the Supporting Information.

dx.doi.org/10.1021/cs500056u | ACS Catal. 2014, 4, 1274−1278

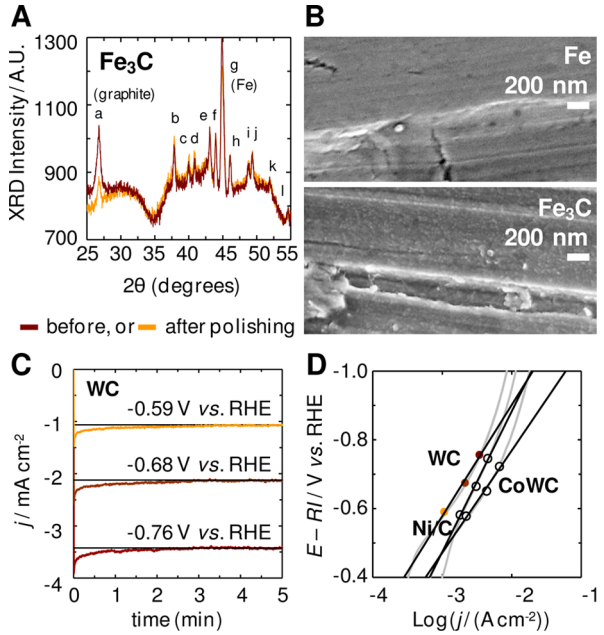

Figure 3. H^+ reduction activity of metal carbide electrodes. Representative (A) XRD pattern of Fe_3C before and after abrasive polishing [a–l mark (020), (121), (002), (201), (211), (102), (031), (112), (131), (221), (122), and (230) facets of Fe_3C, respectively; ref ICDD 00-035-0772],[42] (B) SEM images of Fe before (Fe) and after (Fe_3C) carburization, (C) polarization curves of WC (solid black lines mark the steady-state values), and (D) Tafel plots (dots and linear fits with black lines) and related cyclic voltammograms (light gray) in 0.05 M K_2CO_3 (pH 11.3) at 19 ± 1 °C.

A plot of the experimental exchange current densities as a function of the calculated hydrogen binding energies is shown in Figure 4. The values of i_0 and $\Delta G_B[H]$ for fcc(111) metals and bcc(110) Mo, W, Nb,[12,14] and metal overlayers,[13] i_0 for

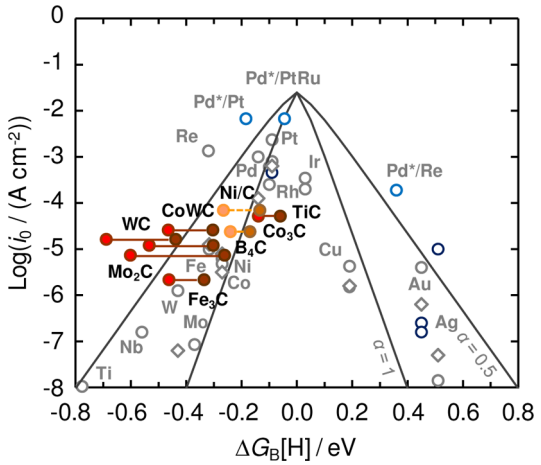

Figure 4. Volcano plot for the HER on polycrystalline (gray circles) or single-crystal (dark blue circles) transition metals (1/4 ML_H) from refs 12, 25, 39, 43, and 44 and Pd overlayers (denoted with Pd*/substrate, light blue circles, 1/4 to 1/3 ML_H) from ref 13 in acidic electrolytes or transition metals in alkaline electrolytes (gray diamonds)[14] and metal carbides in an alkaline electrolyte at 1/6 to 1/4 ML_H (red circles) or 1/3 to 1/2 ML_H (brown circles), connected with a solid line as a guide to the eye. The two solid curved lines show a microkinetic model, assuming transfer coefficients (α) of 0.5 and 1.0, as in refs 12 and 13. All data for metal carbides are provided in the Supporting Information.

Fe[43] and Ti,[44] and $\Delta G_B[H]$ for Fe(111)[39] and Ti($11\bar{2}2$)[25] were compiled from the literature. To search for an approximate trend, the adsorption energies of fcc(211) Ni and Co[13,26,38,39] were used to approximate $\Delta G_B[H]$ for Ni/C and Co_3C and the $\Delta G_B[H]$ for CoWC was estimated as the arithmetic average of $\Delta G_B[H]$ for Co(211) and WC(0001). The correlation shows that including the effect of surface coverage yields the expected increasing exchange current density for the HER with weakened hydrogen chemisorption energies on metal carbide surfaces, relative to that of the parent metal surface. Relative to that of the parent metal, a higher coverage of a metal carbide surface with hydrogen adsorbates is plausible given the stronger hydrogen binding of the bare carbide surfaces relative to that of the bare parent metal surfaces. Generally, the activity of metal carbides for catalyzing the HER is intermediate between the low activities exhibited by early transition metals and the maximal activities inherent in Pt and Pt-group metal compounds. For the reverse reaction, we note it is conceivable that metal carbide surfaces are covered with oxygen adatoms[25] under the electrochemical conditions of the HOR that may alter their catalytic activity.[19] Determining the exchange current density of metal carbide electrodes for the HOR in the future would provide insight into the effect of oxygen adatoms on the catalytic activity of metal carbide electrocatalysts.

While this analysis explains general trends in the reactivity of metal carbide surfaces, given the oxophilic nature of these materials[25] a better correlation of experiment and theory may be obtained when including hydroxyl co-adsorbates (from H_2O cleavage)[12] in the calculation of $\Delta G_B[H]$ because these may be expected to be present at the cathode surface under the studied conditions. Also, the data for the HER catalyzed by metal surfaces in alkaline electrolytes (Figure 4) suggest that the overall trend is not significantly altered by the pH of the electrolyte.[14] This can be understood in terms of the adsorption energy scaling (e.g., of OH and H adsorbates) on transition-metal surfaces[38] that have been shown to apply in modified form for metal carbide surfaces, as well[25] (OH/H adsorption energy scaling on metal carbides is shown in the Supporting Information). Thus, independent of the mechanistic details of the HER at the metal carbide surface, the hydrogen chemisorption energy is found to be a useful and single descriptor of the HER on carbide catalysts if the coverage-dependent weakening of hydrogen chemisorption energies is being taken into account.

■ CONCLUSIONS

This work shows that the catalytic activity of monometallic carbide surfaces for the HER is intermediate between the low activities exhibited by early transition metals and the maximal activities inherent in Pt and Pt-group metal compounds. The exchange current density for the HER on metal carbides can be described with the energy of binding of hydrogen to the catalyst surface. Increased HER activities on carbide catalysts relative to their parent metals can be understood with a 3-fold higher sensitivity of metal carbide surfaces to the weakening of hydrogen adsorption due to surface coverage effects relative to transition-metal surfaces. These trends can be potentially useful for the design and understanding of bimetallic carbide electrocatalysts for various electrochemical applications in which the hydrogen evolution–oxidation reactions should be enhanced or suppressed.

dx.doi.org/10.1021/cs500056u | ACS Catal. 2014, 4, 1274–1278

EXPERIMENTAL METHODS

Full details of the synthesis and preparation of the carbide electrodes and measuring H^+ reduction activities are given in the Supporting Information. Fe_3C, Co_3C, Ni/C, Mo_2C, and WC were synthesized via decomposition of CO, CH_4, or C_6H_{14} over metal precursors at 330−1000 K (Mini-Mite Tube Furnace, Lindberg Blue M), following procedures similar to those described in the literature.[45−49] The metal carbides were characterized (only Ni and graphite for Ni/C) with X-ray diffraction (XRD) and grazing incidence X-ray diffraction (GID) (Cu Kα radiation, 2θ range of 20−80°, scan rate of 1°/min, 3° GI angle, D8 Discover, Bruker), energy-dispersive X-ray spectroscopy (EDX), and scanning electron microscopy (SEM) on a LEO 1530 VP Gemini (Zeiss) instrument.

The carbide electrodes were assembled from carbide sheets (as-purchased, as-synthesized, or abrasively polished) or TiC nanoparticle (NP)/Nafion ink dried on carbon fiber paper.[50] Cyclic voltammograms and steady-state polarization curves were recorded using a one-chamber voltammetry cell (99.99% Pt counter and single-junction Ag/AgCl reference electrodes) with 0.05 M K_2CO_3 (pH 11.3, 19 ± 1 °C). Ar (9.0 ± 0.9 mL_{STP} min^{-1}) was used as purge gas analyzed via gas chromatography. No gaseous products (e.g., from conceivable carbide decomposition) other than H_2 and O_2 were detected. Electrochemically polished (at 2 V in 85% H_3PO_4)[51] polycrystalline Cu was used for reference measurements, which yielded a $\log[i_0/(A\ cm^{-2})]$ value of −5.8 ± 0.3, in agreement with the value of −5.8 ± 0.2 reported previously for the HER on Cu in an alkaline electrolyte.[14] Voltages are converted to versus RHE and corrected for the uncompensated solution resistance.

CHEMICALS

Fe (99.9%), Co (99.95%), Ni (99.9%), Mo (99.98%), and W (99.98%) sheets were obtained from ESPI Metals. Cu (99.98%) sheets were obtained from Sigma-Aldrich. B_4C sheets (99.5%, Ceradyne, Inc.), CoWC rods (10% Co, 90% WC, Ultra Carbide, Inc.), and TiC NPs (40 nm, 99%, Nanostructured & Amorphous Materials, Inc.) were gifts or were obtained commercially (purity given on a trace-metal basis). Gases for GC calibration, purge gas, or carbide synthesis were H_2 (500 ppm), CH_4 (500 ppm), C_2H_4 (100 ppm), CO (500 ppm), and CO_2 (300 ppm), all by mole and diluted in air (JJS Technical Service), 15 ppm by mole of various hydrocarbons in N_2 (23470-U, Sigma-Aldrich), 60 mol % CO in N_2 (MESA Specialty Gases & Equipment), and H_2 (5 N), He (5 N), CH_4 (3.7 N), CO (4 N), CO_2 (5 N), Ar (5 N), and 1 vol % UHP O_2 in N_2 (Corp Brothers, Inc.). Acetone (99.7%), hexanes (99.9%), and a 5% aqueous Nafion solution (Ion Power LQ1150) were from Fisher Scientific. 2-Propanol (99.96%) was from Pharmco-Aaper. CH_3OH (99.8%), H_3PO_4 (85%), and NaOH (98.7%) were from Macron Fine Chemicals. $K_2CO_3 \cdot 1.5H_2O$ (98.5%) was from Acros Organics. The aqueous KCl solution (4 M) was from LabChem, Inc. H_2O was deionized (>18.2 MΩ cm and <5 ppb total organic carbon) and degassed (Direct 16, Millipore).

COMPUTATIONAL METHODS

Computational details are given in-depth elsewhere[25] and in the Supporting Information. Surface calculations on periodic facets of rhombohedral B_4C, cubic TiC, (spin-polarized) orthorhombic Fe_3C, orthorhombic Mo_2C, cubic TaC, and hexagonal WC (the phases with dominant XRD and GID signals) were conducted via density functional theory employing the planewave pseudopotential electronic structure code DACAPO in the ASE environment.[52−56] Exchange correlation interactions were treated with the revised Perdew−Burke−Ernzerhof functional of Hammer, Hansen, and Nørskov.[57]

ASSOCIATED CONTENT

Supporting Information

Experimental and computational details, tabulated exchange current densities and hydrogen binding energies, and scaling relation of OH adsorption energies with H adsorption energies on metal carbide surfaces. This material is available free of charge via the Internet at http://pubs.acs.org.

AUTHOR INFORMATION

Corresponding Author

*E-mail: andrew_peterson@brown.edu. Telephone: (401) 863-2153.

Notes

The authors declare no competing financial interest.

ACKNOWLEDGMENTS

We are grateful to Vineeth Venugopal for his assistance with sample analysis. This work was supported financially by a Young Investigator Award from the Office of Naval Research under Grant N00014-12-1-0851. Electronic structure calculations were conducted at the Center for Computation and Visualization, Brown University.

REFERENCES

(1) Spurgeon, J. M.; Walter, M. G.; Zhou, J.; Kohl, P. A.; Lewis, N. S. *Energy Environ. Sci.* **2011**, *4*, 1772−1780.
(2) Smil, V. *Nature* **1999**, *400*, 415.
(3) Klerke, A.; Christensen, C. H.; Nørskov, J. K.; Vegge, T. *J. Mater. Chem.* **2008**, *18*, 2304−2310.
(4) Dietenberger, M.; Anderson, M. *Ind. Eng. Chem. Res.* **2007**, *46*, 8863−8874.
(5) Lu, S.; Pan, J.; Huang, A.; Zhuang, L.; Lu, J. *Proc. Natl. Acad. Sci. U.S.A.* **2008**, *105*, 20611−20614.
(6) Gasteiger, H.; Panels, J.; Yan, S. *J. Power Sources* **2004**, *127*, 162−171.
(7) Jacobson, M. Z.; Colella, W. G.; Golden, D. M. *Science* **2005**, *308*, 1901−1905.
(8) Schlapbach, L.; Zuttel, A. *Nature* **2001**, *414*, 353−358.
(9) Hori, Y. Electrochemical CO_2 Reduction on Metal Electrodes. In *Modern Aspects of Electrochemistry*; Springer: New York, 2008; Vol. *42*, Chapter 3, pp 89−189.
(10) Zhu, W.; Michalsky, R.; Metin, Ö.; Lv, H.; Guo, S.; Wright, C. J.; Sun, X.; Peterson, A. A.; Sun, S. *J. Am. Chem. Soc.* **2013**, *135*, 16833−16836.
(11) Santos, J.; Matos, R.; Trivinho-Strixino, F.; Pereira, E. *Electrochim. Acta* **2007**, *53*, 644−649.
(12) Nørskov, J. K.; Bligaard, T.; Logadottir, A.; Kitchin, J. R.; Chen, J. G.; Pandelov, S.; Stimming, U. *J. Electrochem. Soc.* **2005**, *152*, J23−J26.
(13) Greeley, J.; Jaramillo, T. F.; Bonde, J.; Chorkendorff, I.; Nørskov, J. K. *Nat. Mater.* **2006**, *5*, 909−913.
(14) Sheng, W.; Myint, M.; Chen, J. G.; Yan, Y. *Energy Environ. Sci.* **2013**, *6*, 1509−1512.
(15) Bligaard, T.; Nørskov, J.; Dahl, S.; Matthiesen, J.; Christensen, C.; Sehested, J. *J. Catal.* **2004**, *224*, 206−217.
(16) Marković, N. M.; Ross, P. N. *Surf. Sci. Rep.* **2002**, *45*, 117−229.
(17) Hinnemann, B.; Moses, P. G.; Bonde, J.; Jorgensen, K. P.; Nielsen, J. H.; Horch, S.; Chorkendorff, I.; Nørskov, J. K. *J. Am. Chem. Soc.* **2005**, *127*, 5308−5309.

(18) Jaramillo, T. F.; Jorgensen, K. P.; Bonde, J.; Nielsen, J. H.; Horch, S.; Chorkendorff, I. *Science* **2007**, *317*, 100−102.
(19) Anastasopoulos, A.; Blake, J.; Hayden, B. E. *J. Phys. Chem. C* **2011**, *115*, 19226−19230.
(20) Levy, R. B.; Boudart, M. *Science* **1973**, *181*, 547−549.
(21) Harnisch, F.; Sievers, G.; Schröder, U. *Appl. Catal., B* **2009**, *89*, 455−458.
(22) Sokolsky, D.; Palanker, V.; Baybatyrov, E. *Electrochim. Acta* **1975**, *20*, 71−77.
(23) Vrubel, H.; Hu, X. *Angew. Chem., Int. Ed.* **2012**, *51*, 12703−12706.
(24) Kitchin, J. R.; Nørskov, J. K.; Barteau, M. A.; Chen, J. G. *Catal. Today* **2005**, *105*, 66−73.
(25) Michalsky, R.; Zhang, Y.-J.; Medford, A. J.; Peterson, A. A. *J. Phys. Chem. C*, Manuscript submitted for publication.
(26) Medford, A. J.; Vojvodic, A.; Studt, F.; Abild-Pedersen, F.; Nørskov, J. K. *J. Catal.* **2012**, *290*, 108−117.
(27) Hwu, H. H.; Polizzotti, B. D.; Chen, J. G. *J. Phys. Chem. B* **2001**, *105*, 10045−10053.
(28) Hwu, H. H.; Chen, J. G. *J. Phys. Chem. B* **2003**, *107*, 2029−2039.
(29) Hwu, H. H.; Chen, J. G. *Chem. Rev.* **2005**, *105*, 185−212.
(30) Ham, D. J.; Lee, J. S. *Energies* **2009**, *2*, 873−899.
(31) Dubois, J. L.; Sayama, K.; Arakawa, H. *Chem. Lett.* **1992**, *21*, 5−8.
(32) Kojima, I.; Miyazaki, E.; Yasumori, I. *J. Chem. Soc., Chem. Commun.* **1980**, *212*, 573−574.
(33) Chai, S. H.; Schwartz, V.; Howe, J. Y.; Wang, X.; Kidder, M.; Overbury, S. H.; Dai, S.; Jiang, D. *Microporous Mesoporous Mater.* **2013**, *170*, 141−149.
(34) Liu, P.; Rodriguez, J. A. *J. Phys. Chem. B* **2006**, *110*, 19418−19425.
(35) Vojvodic, A. *Catal. Lett.* **2012**, *142*, 728−735.
(36) Gracia, J.; Prinsloo, F.; Niemantsverdriet, J. *Catal. Lett.* **2009**, *133*, 257−261.
(37) Lowekamp, J. B.; Rohrer, G. S.; Morris Hotsenpiller, P. A.; Bolt, J. D.; Farneth, W. E. *J. Phys. Chem. B* **1998**, *102*, 7323−7327.
(38) Abild-Pedersen, F.; Greeley, J.; Studt, F.; Rossmeisl, J.; Munter, T.; Moses, P.; Skúlason, E.; Bligaard, T.; Nørskov, J. *Phys. Rev. Lett.* **2007**, *99*, 16105.
(39) Wang, S.; Petzold, V.; Tripkovic, V.; Kleis, J.; Howalt, J. G.; Skúlason, E.; Fernández, E. M.; Hvolbæk, B.; Jones, G.; Toftelund, A.; Falsig, H.; Björketun, M.; Studt, F.; Abild-Pedersen, F.; Rossmeisl, J.; Nørskov, J. K.; Bligaard, T. *Phys. Chem. Chem. Phys.* **2011**, *13*, 20760−20765.
(40) Nørskov, J. K.; Rossmeisl, J.; Logadottir, A.; Lindqvist, L.; Kitchin, J. R.; Bligaard, T.; Jonsson, H. *J. Phys. Chem. B* **2004**, *108*, 17886−17892.
(41) Pfnür, H.; Menzel, D. *J. Chem. Phys.* **1983**, *79*, 2400−2410.
(42) U.S. National Bureau of Standards Monograph 2521, 72 (1985).
(43) Crittenden, J. C.; Trussell, R. R.; Hand, D. W.; Howe, K. J.; Tchobanoglous, G. *Water Treatment: Principles and Design*, 2nd ed.; John Wiley and Sons: New York, 2005.
(44) Thomas, N. T.; Nobe, K. *J. Electrochem. Soc.* **1970**, *117*, 622−626.
(45) Park, E.; Ostrovski, O.; Zhang, J.; Thomson, S.; Howe, R. *Metall. Mater. Trans. B* **2001**, *32*, 839−845.
(46) Harris, V. G.; Chen, Y.; Yang, A.; Yoon, S.; Chen, Z.; Geiler, A. L.; Gao, J.; Chinnasamy, C. N.; Lewis, L. H.; Vittoria, C.; Carpenter, E. E.; Carroll, K. J.; Goswami, R.; Willard, M. A.; Kurihara, L.; Gjoka, M.; Kalogirou, O. *J. Phys. D: Appl. Phys.* **2010**, *43*, 165003.
(47) Nagakura, S. *J. Phys. Soc. Jpn.* **1957**, *12*, 482−494.
(48) Weidman, M. C.; Esposito, D. V.; Hsu, Y. C.; Chen, J. G. *J. Power Sources* **2012**, *202*, 11−17.
(49) Weidman, M. C.; Esposito, D. V.; Hsu, I. J.; Chen, J. G. *J. Electrochem. Soc.* **2010**, *157*, F179−F188.
(50) Guo, S.; Dong, S.; Wang, E. *ACS Nano* **2010**, *4*, 547−555.
(51) Hori, Y.; Murata, A.; Takahashi, R. *J. Chem. Soc., Faraday Trans. 1* **1989**, *85*, 2309−2326.
(52) Both ASE and DACAPO are open-source codes freely available from the Department of Physics at the Technical University of Denmark (Kongens Lyngby, Denmark).
(53) Bahn, S. R.; Jacobsen, K. W. *Comput. Sci. Eng.* **2002**, *4*, 56−66.
(54) Vanderbilt, D. *Phys. Rev. B: Solid State* **1990**, *41*, 7892−7895.
(55) Payne, M. C.; Teter, M. P.; Allan, D. C.; Arias, T. A.; Joannopoulos, J. D. *Rev. Mod. Phys.* **1992**, *64*, 1045−1097.
(56) Kresse, G.; Furthmller, J. *Comput. Mater. Sci.* **1996**, *6*, 15−50.
(57) Hammer, B.; Hansen, L. B.; Nørskov, J. K. *Phys. Rev. B: Solid State* **1999**, *59*, 7413−7421.